Modelling and Design Optimization of a Soft-exosuit for Wearable Assistive Devices

Mohamed Irfan Refai[1,2,*], Abdulaziz Y. Alkayas[2,3], Anup Teejo Mathew[3], Federico Renda[3], Thomas George Thuruthel[2]

***Abstract*—Recent advancements in soft-robotic technologies provide a novel paradigm for designing wearable assistive devices (exosuits), making them comfortable, safe, and offering an enhanced range of motion. However, modeling these non-linear actuation technologies is challenging, particularly due to complex interaction mechanics with the body. As a result, current studies often investigate actuation performance in isolation, which leads to poor translation in wearable applications. This work presents the modeling and design optimization of a soft-exosuit for assisting the motion of the index finger. We modelled both the exosuit and finger using a hybrid multibody toolbox and included their interaction mechanics. The optimal exosuit design for maximum bending of the finger joints resulted in a narrow exosuit base thickness compared to its tip. Moreover, we compared the influence of the objective function on the design of the exosuit. Our results show that it is essential to include interaction mechanics when evaluating actuation performance in these scenarios. The proposed modelling approach can be extended to designing optimal exosuits for other joints of interest.**

***Index Terms*—exosuit, design optimization, SoRoSim, human-machine interaction**

I. Introduction

Wearable assistive devices (exos) for the hand and finger can help elderly individuals or those with movement disorders improve their hand function [1]. Designing such exos requires consideration of several factors, including optimal alignment with the target joint to ensure efficient transmission of assistance, and comfortable anchoring to prevent discomfort during use [2].

Finger exoskeletons can be either passive or active, and can be designed using rigid or soft materials [2]. Rigid structures allow better transmission of assistive torques or forces to the user [3]–[8]. Aligning the exoskeleton joint with the biological joint is relatively straightforward, but any misalignment can introduce parasitic resistance and additional inertial effects from the rigid frame during movement [9]. This misalignment may increase the power needed and require complex control strategies to make the exoskeleton transparent when not assisting [10]. Furthermore, rigid components used to interface with the user can lead to discomfort with prolonged use.

Alternatively, advances in soft-robots could be exploited for this purpose. Exoskeletons made from soft materials, or exosuits, offer advantages such as being lightweight, conformable, provide better distribution of forces and cause less discomfort over time. Use of soft materials allows for a lower-profile design, making them more suitable for daily life applications [11]. However, a significant drawback of exosuits is their reduced efficiency in transmitting assistance to the user [11], [12]. The deformation and movement between biological tissues and the exosuit interface can result in energy losses ranging from 25% to 50% [8], [12]. Optimizing exosuit designs can help improve the transmission of assistance to biological joints.

Rigid finger exoskeletons have been designed using either iterative methods or optimization techniques [13]. Research efforts typically focus on improving hand range of motion [3], [5] or optimizing the force applied by the exoskeleton [4], [7], [14]. In contrast, soft exosuits that are cable-driven have mostly been designed iteratively [15], [16]. While a few studies employ finite element modeling techniques to study exosuits, these often neglect the finger-exosuit system as a whole [17], [18], due to the complexity of modeling the soft exosuit and its interactions with the user's finger mechanics.

This work presents a modelling and design optimization framework for a finger and soft-exosuit system considering soft-rigid contact mechanics. Since active exosuits are made from soft materials and employ actuation principles similar to soft robotics, we explored soft-robot modeling literature to model the finger-exosuit system [19], [20]. The system could be modeled as a hybrid multibody structure; with the exosuit modelled as a Cosserat rod, and the finger joints as rigid links with known joint stiffness. This is feasible using the SoRoSim toolbox, which uses a Geometric Variable Strain (GVS) model to define the strain of the exosuit as a Cosserat rod with a finite set of strain basis functions [21], [22]. Moreover, this toolbox enables both static and dynamic analysis of hybrid soft-rigid robots, and allows for the simulation of interaction mechanics between the finger and the exosuit [23].

We perform simulation studies on a planar finger-soft actuator system to understand the relevant modelling considerations for accurate representation while keeping the optimization problem computationally tractable. Both global and gradient-based optimization algorithms were investigated. Our results highlight the importance of design optimization with both the exosuit and user biomechanics in-the-loop, a consideration lacking in current literature.

[1]Department of Biomechanical Engineering, University of Twente, The Netherlands, [2]Department of Computer Science, University College London, The UK, [3]Khalifa University, UAE.
*m.i.mohamedrefai@utwente.nl

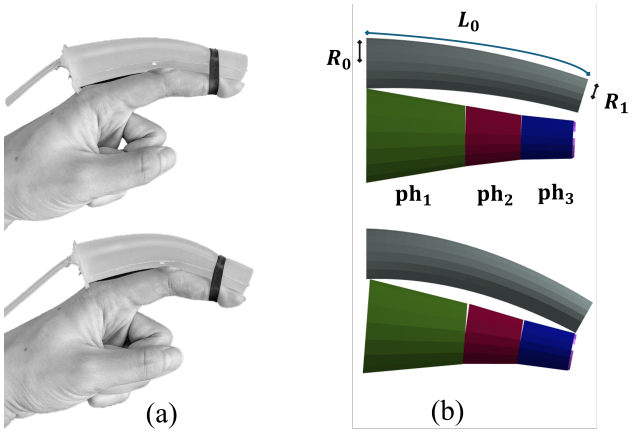

Fig. 1: Modelling the finger-exosuit as seen in (a). The exosuit, modelled with Ecoflex 00-30 (Smooth-On Inc.), was placed parallel to the finger. (b) depicts the model designed using SoRoSim. The exosuit modelled as a soft robot is fixed at the base. The finger consists of three rigid links $ph_1, ph_2,$ and, ph_3, connected via rotational joints (RRR). A tip of negligible thickness is added as a fixed rigid body to ph_3 to increase the number of contact points.

II. Methods

First, we describe the design of the finger-exosuit system using the SoRoSim toolbox in Section II-A, and provide a summary of the implemented underlying model. Following this, we describe the parameter sets of the exosuit that are optimized in Section II-B, the target objectives for optimization in Section II-C, and eventually, the analysis of results in Section II-D.

A. Modelling the finger-exosuit system in SoRoSim

Figure 1a depicts the exosuit worn in parallel with the index finger. The exosuit was fabricated using ecoflex 00-30 silicone (Smooth-On Inc.). The exosuit can be actuated via a chamber positioned at the surface.

1) Kinematics of the exosuit: The soft exosuit was represented using a Cosserat rod model, which conceptualizes the structure as a continuous series of rigid cross-sections described by a curvilinear coordinate $X \in [0, L]$, where L denotes the total length of the rod. A linear Hooke-like elastic law was assumed as the operating values of the systems used would not exceed 100% strains. Therefore, using non-linear material models would not significantly affect our results. The Young's Modulus of the exosuit was set to 30 kPa to resemble Ecoflex properties. By assigning a fixed coordinate frame to each cross-section, the complete configuration of the rod is determined by a directed spatial curve, $\boldsymbol{g}(\bullet) : X \rightarrow \boldsymbol{g}(X) \in SE(3)$, which can be expressed as a homogeneous transformation matrix:

$$\boldsymbol{g}(X) = \begin{bmatrix} \boldsymbol{R} & \boldsymbol{r} \\ \boldsymbol{0}^{1\times 3} & 1 \end{bmatrix}, \tag{1}$$

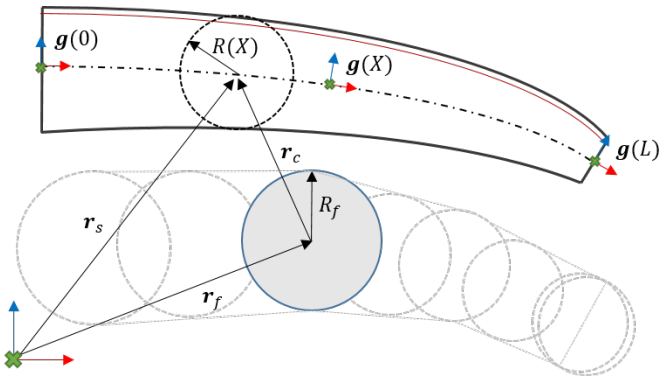

Fig. 2: Schematic of the kinematics and interaction forces of the finger and exosuit in SoRoSim. The exosuit was modelled as a Cosserat rod that can elongate in the X axis and bend around the Y axis. Contact mechanics were defined using spheres placed along the finger and exosuit. The actuation of the exosuit was performed along the red line shown at the surface.

where $\boldsymbol{r}(X) \in \mathbb{R}^3$ represents the position vector of the origin of the moving frame, while $\boldsymbol{R}(X) \in SO(3)$ describes the orientation of the local frame relative to the spatial frame. The local x-axis is oriented perpendicularly to the plane of the cross-section. By differentiating equation (1) with respect to space, denoted by $(\cdot)'$, and time, denoted by $\dot{(\cdot)}$, the following expressions are obtained:

$$\boldsymbol{g}'(X) = \boldsymbol{g}\hat{\boldsymbol{\xi}}; \qquad \dot{\boldsymbol{g}}(X) = \boldsymbol{g}\hat{\boldsymbol{\eta}}. \tag{2}$$

Here, $\hat{\boldsymbol{\xi}}(X)$ describes the strain of the Cosserat rod. Additionally, $\hat{\boldsymbol{\eta}}(X)$ defines the velocity twist, capturing both the translational and rotational velocity of the rod along its length. The operator $\hat{(\bullet)}$ signifies the isomorphism between $\mathbb{R}^6$ and $\mathfrak{se}(3)$. By equating the mixed partial derivatives with respect to space X and time t, the relationship between velocity and strain can be derived, leading to the following result:

$$\boldsymbol{\eta}' = \dot{\boldsymbol{\xi}} - \mathrm{ad}_{\boldsymbol{\xi}}\boldsymbol{\eta}, \tag{3}$$

where, $\mathrm{ad}_{\boldsymbol{\xi}}$ is the adjoint operator of $\boldsymbol{\xi}$.

The integration of equation (2) yields the pose model, while the integration of equation (3) results in the velocity model:

$$\boldsymbol{g}(X) = \exp\left(\widehat{\boldsymbol{\Omega}}(X)\right) \text{ , and} \tag{4}$$

$$\boldsymbol{\eta}(X) = \mathrm{Ad}_{\boldsymbol{g}^{-1}} \int_0^X \mathrm{Ad}_{\boldsymbol{g}}\dot{\boldsymbol{\xi}} ds. \tag{5}$$

Here, $\mathrm{Ad}_{\boldsymbol{g}}$ represents the adjoint form of the homogeneous matrix $\boldsymbol{g}$, while $\boldsymbol{\Omega}$ refers to the Magnus expansion of $\boldsymbol{\xi}(X)$. Next, we move on to discretizing the strain and introducing generalized coordinates. The continuous strain field is simplified into a finite number of strain bases:

$$\boldsymbol{\xi}(X) = \boldsymbol{\Phi}_{\xi}(X)\boldsymbol{q} + \boldsymbol{\xi}^*(X). \tag{6}$$

Here, $\boldsymbol{\Phi}_{\xi}(X) \in \mathbb{R}^{6\times n}$ is the matrix function whose columns define the basis for the strain field, $\boldsymbol{q} \in \mathbb{R}^n$ (where n is the

TABLE I: Design parameters of the finger and exosuit

Item	**Length** (cm)	**Radius Base** (cm)	**Radius Tip** (cm)	**Joint Stiffness** (Nm/rad)
exosuit	10	1.16	0.8	–
ph_1	4.5	2.16	1.39	0.04
ph_2	2.53	1.39	1.02	0.03
ph_3	2.36	1.02	0.87	0.02
tip	0.1	0.87	0.8	–

TABLE II: Parameter sets for optimization

Set	**Parameter Optimized**	**Parameters**
L	length of the exosuit	L
$R_{0,1}$	base and tip radius of the exosuit	[R_0, R_1]
R_{sc}	exosuit surface as a sum of a sine and a cosine wave	[A, B, phi_A, phi_B]
R_{LP}	exosuit surface as a sum of 10 Legendre Polynomials	$a_0, a_1, a_2, ..., a_{10}$

number of generalized coordinates) is the vector of generalized coordinates in that basis, while $\boldsymbol{\xi}^*(X)$ represents the rod's strain in its natural, stress-free state. Substituting equation (6) into equation (3) ultimately leads to the velocity model:

$$\boldsymbol{\eta}(X) = \mathrm{Ad}^{-1}_{\boldsymbol{g}(X)} \int_0^X \mathrm{Ad}_{\boldsymbol{g}} \boldsymbol{\Phi}_\xi ds \dot{\boldsymbol{q}} = \boldsymbol{J}(\boldsymbol{q}, X)\dot{\boldsymbol{q}}. \tag{7}$$

Here, $\boldsymbol{J} \in \mathbb{R}^{6\times n}$ represents the geometric Jacobian. While Equations (4) and (5) are analytical, they cannot be computed directly. A recursive formulation of the kinematic equations, using a quadrature approximation of the Magnus expansion $\boldsymbol{\Omega}$, is provided in [24], [25].

The exosuit uses a nodal basis reminiscent to the quadratic basis of FEM with 3 quadrature points [24]. The degrees of freedom of the exosuit was constrained such that it could extend in the local X axis and bend about the Y axis.

2) Kinematics of the finger: We assumed the finger to be passive, and modelled it as a rigid three bar linkage with rotational joints (RRR). The dimensions and joint stiffness are derived from literature [26]–[28]. The modeling of the linkage follow the classical rigid robot modeling [29] with the addition of external loads defined by the contact forces. We consider more contact points at the tip realized by an additional fixed link with negligible length (see Sec. II-A3).

The dimensions of the finger-exosuit system are provided in Table I. The finger-exosuit system has 25 degrees of freedom in total. 22 of these define the kinematics of the exosuit, and three denote the rotation of the finger joints. The rotation of the first finger joint was constrained between -10° and 90° whereas the second and third were constrained between -5° and 90°.

3) Contact forces: To model the interaction between the exosuit and the finger, we implement a simple interference contact model, approximating the contact as between two spherical bodies, as shown in Fig. 2. The contact model is defined by the following:

$$\boldsymbol{f}_c = \begin{cases} kd\dfrac{\boldsymbol{r}_c}{\|\boldsymbol{r}_c\|} & \text{if } d > 0 \\ 0 & \text{if } d < 0 \end{cases}, \tag{8}$$

where $\boldsymbol{r}_c = \boldsymbol{r}_s - \boldsymbol{r}_f$, $d = R_f + R(X) - \|\boldsymbol{r}_c\|$ (see Fig. 2 for details) and k is the contact stiffness of the model. Note that the contact force model only has a normal component. For the sake of simplicity, we ignore the tangential friction. The exosuit had 42 contact spheres defined along its length, whereas the finger had eight contact spheres. The static equilibrium for the system is solved, accounting for contact interactions between the finger and the exosuit.

4) Statics: By projecting the static equilibrium equations of the soft exosuit [22] and the rigid finger into the space of generalized coordinates using the geometric Jacobian through D'Alambert's principle, we get the generalized static equation:

$$\boldsymbol{K}\boldsymbol{q} = \boldsymbol{B}(\boldsymbol{q})u + \boldsymbol{F}(\boldsymbol{q}), \tag{9}$$

where $\boldsymbol{K} \in \mathbb{R}^{n\times n}$ is the stiffness matrix, $\boldsymbol{B}(\boldsymbol{q}) \in \mathbb{R}^n$ is the actuation matrix, u is the actuation force due to the pneumatic chamber represented as the red line in Fig. 2 and $\boldsymbol{F}(\boldsymbol{q}) \in \mathbb{R}^n$ is the vector of generalized external (contact) forces.

To implement and solve the full system model, we execute root-finding methods for equation (9). By incrementally increasing the actuation force and using each equilibrium solution as the initial guess for the next iteration, the system progressively adjusts to maintain stability and computational efficiency as the load increases.

B. Exosuit Parameter Sets

The parameters considered for optimization included the length (L) and the shape of the exosuit surface ($S(X)$). Table II summarizes the parameters, including the three approaches used to model $S(X)$. Their respective formulations are:

$$R_{0,1} : S(X) = R_0 + X/L \cdot (R_1 - R_0), \tag{10}$$

$$R_{sc} : S(X) = R_0 + \frac{R_0}{20}(sin(A \cdot \pi \cdot X/L + \phi_A) + cos(B \cdot \pi \cdot X/L + \phi_B)), \text{and,} \tag{11}$$

$$R_{LP} : S(X) = \sum_{n=0}^{N-1} A_{n+1} P_n(X). \tag{12}$$

Equation (10) models $S(X)$ linearly from the base (R_0) to tip (R_1) of the exosuit. Thus, for this case $R_{0,1}$, there are two parameters to be optimized (Table II). Equation (11) denotes the formulation for R_{sc}, where $S(X)$ is defined as the sum of a sine and a cosine wave. For this set, there are four parameters to optimize; the frequency (A, B) and phase (phi_1, phi_2) of the respective waves. Finally, R_{LP} in equation (12) denotes the surface as a sum of $N-1$ Legendre Polynomials (LP) of degree n ($P_n(X)$). Here, the amplitude of the LPs of subsequent degrees decreases as $A_{n+1} = \frac{2a_n}{3^n}$, where a_n denotes the n-th LP. To prevent very small exosuit thickness, the minimum radius of the exosuit was limited to 0.5 cm. We optimized either the length, the $S(X)$, or both length and $S(X)$.

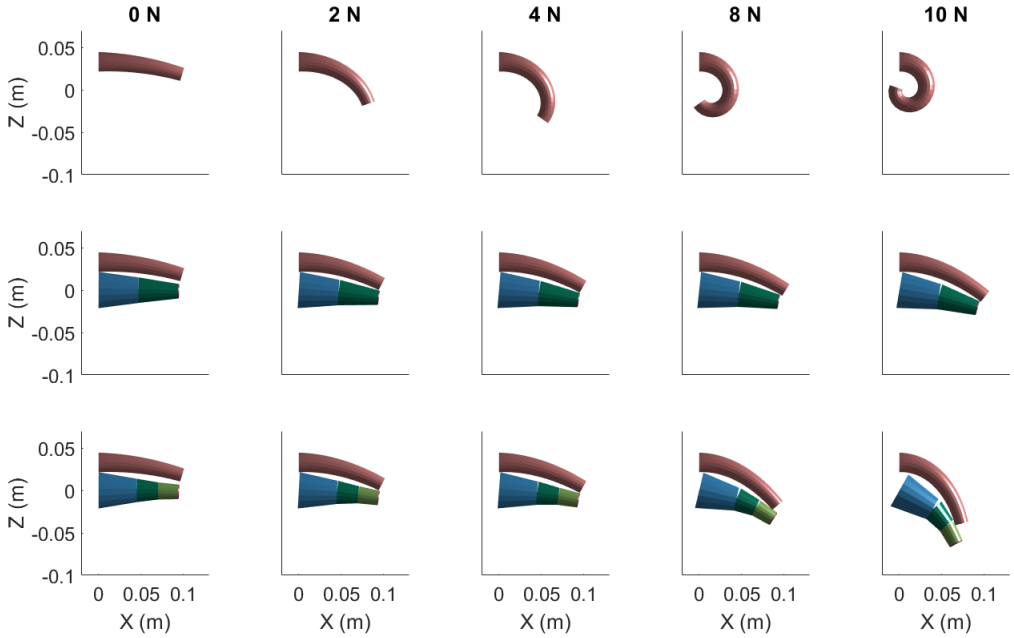

Fig. 3: The exosuit was actuated from 0 N to 10 N in steps of 2 N. In the second and third rows, we demonstrate the interaction of the exosuit with a simulated finger defined using either two or three rigid links respectively, showing the effect of interaction dynamics on overall behavior. The exosuit could only elongate in the X-axis and bend in the Y-axis.

C. Optimization objectives

Hand exos are optimized for their force transmission or resulting range of motion of the fingers [2]–[5], [7], [15], [16], [30]. Therefore, we identified objective functions that target either the deformation or forces applied to the finger:

$$f_b = ||\mathbf{q}_b||, \quad (13)$$

$$f_{exo} = -F_t, \text{and} \quad (14)$$

$$f_{bc} = ||\mathbf{q}_{bc}||. \quad (15)$$

The first objective function (13), f_b, maximizes the bending of the three finger joints by minimizing $\mathbf{q}_b$, where $\mathbf{q}_b = [\pi - \theta_1,\ \pi - \theta_2,\ \pi - \theta_3]^T$, with θ_1, θ_2, and θ_3 representing the bending angles of the finger joints. The objective function f_{exo} in equation (14) maximizes the force F_t applied by the tip of the exosuit on the finger. Finally, we wanted to maximize the bending of the finger while ensuring that the exosuit tip did not slide along the finger. Therefore, f_{bc} in equation (15) included the number of spheres along the exosuit that were in contact with the finger (n_c) to the objective function. Here, $\mathbf{q}_{bc}$ is defined as $[\mathbf{q}_b, -n_c]^T$. In all cases, the exosuit was actuated with force increments starting from 0 N in steps of 1 N, and the objective functions were evaluated when the actuation reached 5 N.

D. Analysis of Results

First, we demonstrate how the configuration of the default finger-exosuit system changed with increasing exosuit actuation. Next, we evaluate the performance of both gradient-based and non-gradient-based optimization algorithms for optimizing the system's parameters. The gradient-based algorithms were executed using standard approaches in MATLAB, whereas, we utilized MATLAB's parallel computing toolbox for the non-gradient-based algorithms. We then present the optimal parameters identified for each parameter set, followed by an analysis of how different objective functions influence the resulting optimal parameters. The simulations and optimizations were performed using MATLAB R2024a on a Windows 11 PC with 16 GB RAM and a 6-core processor clocked at 3.4 GHz.

TABLE III: Optimized values for each parameter set

Set	**Optimized Values**	**Time** (min)
L	7.97 cm	30
$R_{0,1}$	[0.67, 0.75] cm	96
L, $R_{0,1}$	[10.8, 0.65, 0.74] cm	201
R_{sc}	[-2, -0.5, 0, 0]	66
L, R_{sc}	10 cm, [-2, -0.5, 0, 0]	77
R_{LP}	[0.4, 0.7, 0, 1, 0.8, 0.9, 1, 1, 1, 1]	236
L, R_{LP}	10 cm; [0.4, 0.7, 0, 1, 0.8, 0.9, 1, 1, 1, 1]	264

III. Results

In Fig. 3, we illustrate the differences in exosuit actuation with and without the finger. In the second row, we introduce an intermediary design where the finger is modeled with two rigid links, to demonstrate changes in the exosuit kinematics with respect to degrees of freedom of the finger. The exosuit was actuated with forces ranging from 0 to 10 N in increments of 2 N. The current kinematic state of the finger-exosuit system was used as the initial condition for solving the subsequent

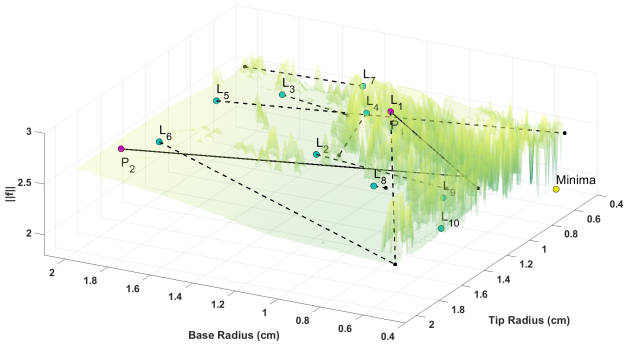

(a)

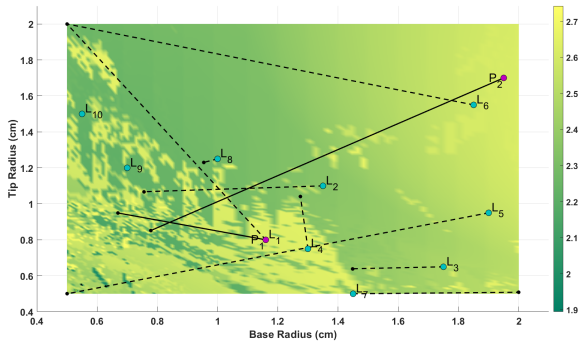

(b)

Fig. 4: Optimization of set $R_{0,1}$ using non-linear least-squares (LS) and pattern search (PS) algorithms. (a) and (b) show two different views of the non-linear solution space, with the global minima depicted in (a). The 10 and 2 random initial conditions for LS and PS are denoted with L_i and P_i respectively.

actuation step. At 10 N, the sum of angles of the finger joints was 0.27 rad with two links, whereas with three links, the bending increased to 1.05 rad. As the finger and exosuit tips were not kinematically fixed in the implemented SoRoSim model, the exosuit slid along the finger as bending and actuation increased.

Next, we evaluated the performance of gradient-based and non-gradient-based algorithms in optimizing the exosuit parameters. Fig. 4 illustrates that the value of the objective function f_b for the set $R_{0,1}$ (which includes the radii at the base and tip of the exosuit) varies non-linearly. We compared the performance of the non-linear least squares solver (LS) implementing Levenberg-Marquadt and pattern-search (PS) algorithms in identifying the global minimum. The true global minimum is shown in yellow in Fig. 4a where R_0 and R_1 are 0.53 cm and 0.52 cm respectively. Ten random initial conditions were used for LS, while two were used for PS. Based on the results, we proceeded with the PS algorithm for further analysis.

Table III presents the values for each parameter set of the exosuit optimized for maximum finger bending (f_b in equation (13)). The resulting exosuit designs are visualized

TABLE IV: Optimal values of $(L,\ R_{0,1})$ set for each Objective Function

Objective Function	L (cm)	R_0 (cm)	R_1 (cm)	**Time** (min)
f_b	10.8	0.65	0.74	203
f_{exo}	10.4	0.62	0.80	119
f_{bc}	9.6	0.88	0.57	166

in Fig. 5. For each set, the exosuit was actuated from 0 to 5 N in 1 N increments. In Fig. 5, we show the kinematics of the finger-exosuit system at 0 and 5 N. Since the objective was to maximize finger bending at 5 N, all optimized parameter sets outperformed the default model parameters. Optimizing the $(L,\ R_{LP})$ parameter set took the longest, while the $(L,\ R_{0,1})$ set achieved the furthest finger bending, reaching 1.43 rad when actuated with 5 N.

Fig. 6 compares the differences in bending of the finger joints for the three objective functions chosen (equation (13) - (15)). We present results for the parameter set $(L,\ R_{0,1})$ as it had the most bending among all sets (Fig. 5). We find that all three objective functions enabled bending of the finger joints. Table IV summarizes the optimal values of L, R_0, and R_1 for each objective function, and the time taken for the optimization.

IV. Discussion

In this paper, we present the modeling and design optimization of a soft exosuit for the finger. Utilizing SoRoSim toolbox allowed us to include both soft-exosuit and finger mechanics in-the-loop. We simulated the exosuit as a planar pneumatic actuator and included simple interaction mechanics between the finger and exosuit during movement. This model was used to optimize the design of the exosuit to maximize the range of motion of the finger. This study offers a simulation-based approach for designing a soft exosuit for the finger, with potential to inform optimal designs for other soft wearable assistive devices.

Fig. 4 shows that the bending of finger joints does not change smoothly as the base and tip radius of the exosuit is changed. Moreover, the global minima was found to be around 0.53 cm and 0.52 cm for the R_0 and R_1 respectively, and not at the lower bounds of the radii (0.4 cm). This could be due to possible sliding of the exosuit tip over the finger which results in a non-linear change in the objective function as a function of change in the exosuit radii.

As we modelled the exosuit as a Cosserat Rod, the parameters to be optimized varied from 1 (set L) to 11 (set $(L,\ R_{LP})$). Nonetheless, this is close to or lower than studies that optimize rigid finger exos which include 10 to 21 parameters [4], [7], [14]. While evolutionary algorithms are commonly used for exosuit design optimization [13], a preliminary comparison with other non-gradient-based algorithms revealed that pattern search (PS) was most robust in converging to an optimal solution. Although, utilizing the parallel computing toolbox reduced the overall optimization time, optimizing the $(L,\ R_{LP})$ parameter set still took nearly

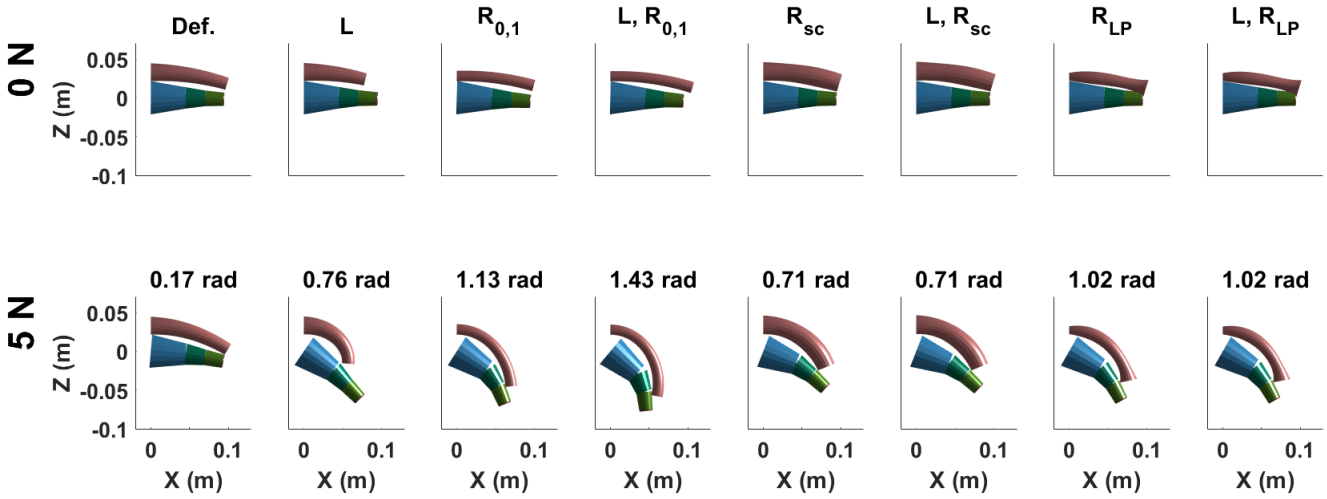

Fig. 5: Initial and final kinematics of the finger-exosuit system for each parameter set. The parameters optimized include length of the exosuit (L) and its shape (S(X)). S(X) was defined using either the initial and final radii ($R_{0,1}$), or as the sum of a sine and cosine wave (R_{sc}), or as the sum of 10 Legendre Polynomials (R_{LP})).

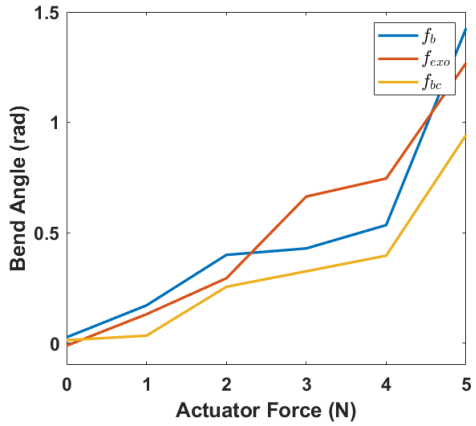

Fig. 6: The differences in bending angle across the three objective functions for the $(L,\ R_{0,1})$ set are shown. The exosuit is actuated from 0 N to 5 N.

4.5 hours. R_{LP} (equation (12)) defined the exosuit surface as a general spline, however, this parameter set did not result in most bending of the joints. This could have been due to inability of the PS to converge to a global minimum for this set with 11 parameters. Advanced optimization algorithms could explore the higher dimension solutions space more efficiently.

The overall bending for the parameter set $(L,\ R_{0,1})$ at 5 N was 82° (Fig. 5). The pose of the finger shows that although the exosuit bends the finger joints, unlike rigid exos, it is not able to curl the fingers [4]. This is mainly due to the design of the exosuit actuation. Inclusion of additional chambers could help target different finger poses including curling.

As the actuator is placed along the surface of the exosuit, changing the exosuit parameters influences the force transmission, and in turn contact with the finger. In Fig. 5, we see for all three cases ($R_{0,1}$, R_{sc}, and, R_{LP}), that the optimal exosuit surface is shaped with a thinner base and a thicker tip. As the exosuit is actuated, the thinner base allows greater bending, resulting in the exosuit sliding across the finger. This effect arises from the lack of a fixed joint between the finger and the exosuit. Additionally, Table III shows that for parameter sets with more complex surface definitions ($(L,\ R_{sc})$ and $(L,\ R_{LP})$), the parameter L remains close to its initial value. This suggests that the shape of the exosuit surface has a greater impact on bending than its length. Nonetheless, including a constraint between the tips of the exosuit and the finger could influence the mechanics of the finger-exosuit system and thereby the optimal design of the exosuit [3]–[5], [7], [14]. This constraint was excluded in this study as it prevented a natural bending of the finger with increasing actuation of the exosuit.

We evaluated the impact of different objective functions on the optimization of the parameter sets in Fig. 6 and Table IV. Overall, the objective function focused on maximizing bending was the most effective. The parameter values of L, R_0, and R_1 were similar for the objective functions f_b and f_{exo}. For both cases, the base radius R_0 was smaller than the tip radius R_1, and they both have a large bend angle of the finger when the exosuit was actuated to 5 N (Fig. 6). Alternatively, f_{bc} resulted in a narrower tip in order to maximise contact between the exosuit and the finger.

There are a few limitations to the study. We assumed a simple contact model with only normal contact forces. Incorporating tangential friction and velocity-dependent interactions could enhance the interaction mechanics between the finger and the exosuit, but would require more robust solvers that account for kinematic and closed loop constraints in the finger-

exosuit system [31]. This would help us analyze the interaction between the exosuit and finger in further detail.

We modeled the finger using average dimensions measured from participants [26]–[28]. However, the lengths of the finger segments could have also been varied to study the changes in optimal exosuit design for varying anthropometry [7]. Moreover, we focused on exosuits that are placed in parallel to the finger, whereas, soft-exosuits typically wrap around the finger [15], [16], [30]. This requires modelling the exosuit as a glove and modelling additional interactions with the finger. Finally, the finger was assumed to be a three rigid link system passively driven with fixed joint stiffness. Biomechanical simulation tools that incorporate the musculoskeletal structures can offer better insights on the user biomechanics during movement [32].

As a follow-up, the results from the simulation must be compared to experimental data. The optimal exosuit design can be fabricated using Ecoflex and actuated to assist a 3D printed finger [33]. The elongation and bending of the exosuit needs to be constrained to match the simulation presented in this study. This can help us validate the optimal exosuit designs identified by the technique.

V. Acknowledgement

This work was partly supported by the Netherlands Sectorplan Techniek 2 and the Royal Society research grant RGS/R1/231472. The authors thank Yunqi Huang for fabricating the exosuit.

References

[1] Z. Jiryaei and A. S. Jafarpisheh, "The usefulness of assistive soft robotics in the rehabilitation of patients with hand impairment: A systematic review," pp. 398–409, 7 2024.

[2] T. du Plessis, K. Djouani, and C. Oosthuizen, "A review of active hand exoskeletons for rehabilitation and assistance," *Robotics*, vol. 10, 2021.

[3] R. Liang, G. Xu, B. He, M. Li, Z. Teng, and S. Zhang, "Developing of a rigid-compliant finger joint exoskeleton using topology optimization method," in *Proceedings - IEEE ICRA*, 2021.

[4] H. Li, L. Cheng, N. Sun, and R. Cao, "Design and control of an underactuated finger exoskeleton for assisting activities of daily living," *IEEE/ASME T. Mech.*, vol. 27, pp. 2699–2709, 2022.

[5] C. J. Haarman, E. E. Hekman, J. S. Rietman, and H. V. D. Kooij, "Mechanical design and feasibility of a finger exoskeleton to support finger extension of severely affected stroke patients," *IEEE TNSRE*, vol. 31, pp. 1268–1276, 2023.

[6] D. Scherb, S. Wartzack, and J. Miehling, "Modelling the interaction between wearable assistive devices and digital human models—a systematic review," *Front. Bioeng. Biotech.*, vol. 10, pp. 1–11, 2023.

[7] B. Akbas, H. T. Yuksel, A. Soylemez, M. Sarac, and F. Stroppa, "Enhanced optimization strategies to design an underactuated hand exoskeleton," 8 2024. [Online]. Available: http://arxiv.org/abs/2408.07384

[8] S. N. Yousaf, G. Mukherjee, R. King, and A. D. Deshpande, "Experimental and simulation-based estimation of interface power during physical human-robot interaction in hand exoskeletons," *IEEE Robotics and Automation Letters*, vol. 9, pp. 2575–2581, 3 2024.

[9] A. T. Asbeck, S. M. D. Rossi, I. Galiana, Y. Ding, and C. J. Walsh, "Stronger, smarter, softer: Next-generation wearable robots," *IEEE Robotics and Automation Magazine*, vol. 21, pp. 22–33, 2014.

[10] A. Stienen, E. Hekman, F. van der Helm, and H. van der Kooij, "Self-aligning exoskeleton axes through decoupling of joint rotations and translations," *IEEE TRO*, vol. 25, pp. 628–633, 6 2009.

[11] C. Thalman and P. Artemiadis, "A review of soft wearable robots that provide active assistance: Trends, common actuation methods, fabrication, and applications," *Wearable Technologies*, vol. 1, pp. 1–27, 2020.

[12] M. B. Yandell, B. T. Quinlivan, D. Popov, C. Walsh, and K. E. Zelik, "Physical interface dynamics alter how robotic exosuits augment human movement: implications for optimizing wearable assistive devices," *JNER*, vol. 14, 2017.

[13] F. Stroppa, A. Soylemez, H. T. Yuksel, B. Akbas, and M. Sarac, "Optimizing exoskeleton design with evolutionary computation: An intensive survey," *Robotics*, vol. 12, 8 2023.

[14] D. Chakraborty, A. Rathi, and R. Singh, "Design and evaluation of exoskeleton device for rehabilitation of index finger using nature-inspired algorithms," *Applied Intelligence*, vol. 54, 2024.

[15] F. Klug, M. Hessinger, T. Koka, P. Witulla, C. Will, T. Schlichting, C. Endl, A. Albenstetter, P.-O. Champagne, D. H. Gagnon, and M. Kupnik, "An anthropomorphic soft exosuit for hand rehabilitation," in *2019 IEEE 16th ICORR*, 6 2019, pp. 1121–1126.

[16] Q. Sanders and D. J. Reinkensmeyer, "Design and preliminary evaluation of a soft finger exoskeleton controlled by isometric grip force," *Machines*, vol. 12, 4 2024.

[17] T. Bagneschi, D. Chiaradia, G. Righi, G. D. Popolo, A. Frisoli, and D. Leonardis, "A soft hand exoskeleton with a novel tendon layout to improve stable wearing in grasping assistance," *IEEE Transactions on Haptics*, vol. 16, pp. 311–321, 4 2023.

[18] J. V. McCall, G. D. Buckner, and D. G. Kamper, "Soft pneumatic actuators for pushing fingers into extension," *JNER*, vol. 21, 12 2024.

[19] C. Laschi, T. G. Thuruthel, F. Lida, R. Merzouki, and E. Falotico, "Learning-based control strategies for soft robots: Theory, achievements, and future challenges," *IEEE Control Systems*, vol. 43, 2023.

[20] C. D. Santina, C. Duriez, and D. Rus, "Model-based control of soft robots: A survey of the state of the art and open challenges," *IEEE Control Systems*, pp. 30–65, 6 2023.

[21] F. Boyer, V. Lebastard, F. Candelier, and F. Renda, "Dynamics of continuum and soft robots: A strain parameterization based approach," *IEEE Transactions on Robotics*, vol. 37, no. 3, pp. 847–863, 2020.

[22] F. Renda, C. Armanini, V. Lebastard, F. Candelier, and F. Boyer, "A geometric variable-strain approach for static modeling of soft manipulators with tendon and fluidic actuation," *IEEE Robotics and Automation Letters*, vol. 5, no. 3, pp. 4006–4013, 2020.

[23] A. T. Mathew, I. B. Hmida, C. Armanini, F. Boyer, and F. Renda, "Sorosim: A matlab toolbox for hybrid rigid–soft robots based on the geometric variable-strain approach," *IEEE Robotics & Automation Magazine*, vol. 30, no. 3, pp. 106–122, 2023.

[24] A. T. Mathew, D. Feliu-Talegon, A. Y. Alkayas, F. Boyer, and F. Renda, "Reduced order modeling of hybrid soft-rigid robots using global, local, and state-dependent strain parameterization," *IJER*, 2025.

[25] F. Renda, C. Armanini, A. Mathew, and F. Boyer, "Geometrically-exact inverse kinematic control of soft manipulators with general threadlike actuators' routing," *IEEE Robotics and Automation Letters*, vol. 7, no. 3, pp. 7311–7318, 2022.

[26] E. Dionysian, J. M. Kabo, F. J. Dorey, and R. A. Meals, "Proximal interphalangeal joint stiffness: Measurement and analysis," *Journal of Hand Surgery*, vol. 30, pp. 573–579, 5 2005.

[27] P. H. Kuo and A. D. Deshpande, "Muscle-tendon units provide limited contributions to the passive stiffness of the index finger metacarpophalangeal joint," *J. Biomech.*, vol. 45, pp. 2531–2538, 10 2012.

[28] X. Q. Shi, H. L. Heung, Z. Q. Tang, K. Y. Tong, and Z. Li, "Verification of finger joint stiffness estimation method with soft robotic actuator," *Frontiers in Bioengineering and Biotechnology*, vol. 8, 12 2020.

[29] K. M. Lynch and F. C. Park, *Modern Robotics: Mechanics, Planning, and Control*. Cambridge University Press, 2017.

[30] X. Xiong and P. Manoonpong, "A variable soft finger exoskeleton for quantifying fatigue-induced mechanical impedance," in *Proceedings - IEEE International Conference on Robotics and Automation*, 2021.

[31] P. Flores, "Contact mechanics for dynamical systems: a comprehensive review," pp. 127–177, 2 2022.

[32] V. Caggiano, H. Wang, G. Durandau, M. Sartori, and V. Kumar, "Myosuite – a contact-rich simulation suite for musculoskeletal motor control," 2022. [Online]. Available: http://arxiv.org/abs/2205.13600

[33] J. ten Kate, G. Smit, and P. Breedveld, "3d-printed upper limb prostheses: a review," *Disability and Rehabilitation: Assistive Technology*, vol. 12, pp. 300–314, 4 2017.